Highly dynamic locomotion control of biped robot with swing arms

Weijie Wang[1], Song Liu[2], Qinfeng Shan[3] and Lihao Jia[*]

***Abstract*— The swinging motion of the arms plays a crucial role in improving the dynamic movement of humans by expanding their ability to control angular momentum, as viewed through the lens of biomechanics. However, biped robot with human morphological structures rarely take full advantage of the swing arms, since there is no effective locomotion control strategy combining swing arms modeling and control reasonably suitable. In this paper, a control strategy is proposed for bipedal robots that incorporates swing arms in the process of achieving jumping motion. The strategy involves modeling, planning trajectories, and tracking movements to enhance the overall performance and stability of the robot. In this process, in order to extract characteristics of swing arms, biped robot is modeled as a flywheel-spring loaded inverted pendulum (F-SLIP), and whole-body controller (WBC) is chosen as the method of trajectory tracking to bring these characteristics into play. Simulation of jumping motion is implemented on a kind of biped robot Purple V1.0 designed for high explosive locomotion, and an well-established evaluation method of biped robot's highly dynamic locomotion is proposed which includes three aspects of agility, stability and energy consumption. Experiment results show this control strategy's effectiveness: agility is increased by a maximum of 6%, stability is enhanced by an average of 30%, and energy consumption is reduced by an average of 15%.**

I. INTRODUCTION

Due to its unique discrete ground support characteristic, bipedal robots are better suited for navigating challenging surroundings compared to customary tracked or mobilized robots. Jumping motion is a fundamental aspect of enabling highly dynamic locomotion in bipedal robots in various contexts. Achieving a stable, agile, and efficient jumping motion in bipedal robots has been a topic of long-standing interest, but remains a challenging problem to address. During the 1980s, Raibert proposed a control strategy for legged robots that enabled jumping motion. This strategy divided jumping motion into three stages - hopping, moving forward, as well as body rotation - each of which were controlled independently [1] [2]. This control strategy is considered to be pivotal in the development of legged robots. In recent decades, numerous advanced control strategies have emerged for legged robots, with a common approach being the use of the simplified model of the spring-loaded inverted pendulum (SLIP) [3] to plan the COM's (center of mass) motion for the bipedal robot, and this is then followed by the design of a joint controller that can track the COM trajectory to complete some motion [4] [5]. In addition, there exist control methods that utilize the momentum principle to directly plan the trajectory of the joints, followed by the design of a corresponding joint controller to ensure efficient tracking of the joint trajectory [6] [7].

While classic control strategies for dynamic locomotion are effective, they do not account for the role of swing arms. Numerous investigations in biomechanics reveal that the integration of swing arms may improve the efficacy of jumping movements across three primary domains:

1) Increasing the jumping agility, which is caused by the increase of plantar forces at the moment of takeoff due to the release of energy stored in swing arms [8] [9].
2) Improving landing stability induced by the compensation of body rotational angular momentum resulting from swing arms [10] [11].
3) Lowering energy consumption due to the introduction of swing arms, which reduce the load of lower limbs [11] [12].

In light of these effects of swing arms, some research teams begin to design human-like biped robot and study swing arms effects. However, most of them just conduct the study based on non-highly dynamic locomotion [13] [14], such as keeping posture stability and increasing movement speed. Regardless of a few of groups of researchers analyzing what swing arms do in highly dynamic locomotion, swing arms are still not given sufficient consideration in modeling, and swing arm trajectories are created manually. [15]. As a result, the impacts of swing arms during biped robots' highly dynamic locomotion have not yet been thoroughly or systematically examined.

To sum up, considering the importance of swing arms in biped robot motion and the lack of exploration in this field, this paper introduces the following key contributions:

- A kind of control strategy of biped robot locomotion that is extremely dynamic utilizing swing arms is proposed. In modeling, by considering swing arms as equivalent to a flywheel, we can derive a simplified representation of F-SLIP [16] that effectively captures the unique features of swing arms. In trajectory planning, by utilizing F-SLIP as the underlying model, we developed a trajectory planning approach for jumping motions that fully integrates the effects of swinging arms. In trajectory tracking, we opted for the Whole Body Control (WBC) method, which enables us to track the complete motion trajectory, generating appropriate joint control inputs that are intelligent and tailored to different control tasks [17].

W.Wang, Song Liu, Q.Shan, and L.Jia are with the Research Center for Brain-inspired Intelligence, Institute of Automation, Chinese Academy of Sciences, Beijing 100190 China and Centre for Artificial Intelligence and Robotics, Hong Kong Institute of Science & Innovation, Chinese Academy of Sciences. Q.Shan and W.Wang are also with the School of Artificial Intelligence, University of Chinese Academy of Sciences, Beijing 100049 China. e-mail:wangweijie2020@ia.ac.cn.

*Corresponding author is Lihao Jia.

This work was supported by the Natural Science Foundation of China (Grant No. 61933001 and 61903361)

- A kind of evaluation method of biped robot's highly dynamic locomotion which includes agility and stability indicators, which are firstly proposed by us, as well as energy consumption indicator.

The paper's rest will be structured as follows. Section II provides this overview of the F-SLIP and dynamics model of the biped robot Purple V1.0. Section III discusses the desired planning of the robot's jumping motion trajectory, which is based on the F-SLIP model. Section IV describes the design of the WBC to monitor the trajectory of the jumping motion. Section V displays the simulation's results and corresponding analyses. Finally, Section VI provides the conclusions and outlines areas for future research.

II. Modeling

This section introduces both the simplified planning model, F-SLIP, and the comprehensive dynamics model of Purple V1.0.

A. The F-SLIP Model

The F-SLIP model is an extension of the existing SLIP model [3] that includes a flywheel which is set on the mass, as illustrated in Figure 1. The F-SLIP model incorporates a flywheel into its centroidal dynamics, which maintains the point mass dynamics and can effectively capture the hopping characteristics of robot's COM. A detailed description of the dynamics is provided below:

$$m\ddot{\boldsymbol{x}} = -\boldsymbol{F}_g + \frac{\tau}{r}[-cos\beta, sin\beta]^T + \boldsymbol{F}_s \tag{1}$$

$$||\boldsymbol{F}_s|| = k\,(r_0 - r) \tag{2}$$

$$I\ddot{\theta} = \tau \tag{3}$$

where $\boldsymbol{x} = [x, z]^T$, x and z represents the horizontal and vertical position of COM respectively; $\boldsymbol{F}_g = [0, mg]^T$, m represents robots' overall weight, g represents gravitational constant; $\boldsymbol{F}_s = [F_{s_x}, F_{s_z}]^T$, F_{s_x}, F_{s_z} represent the horizontal and perpendicular components of spring force respectively; k is the stiffness of the spring; I represents flywheel's rotational inertia; τ represents the torque acting on the flywheel; θ represents the flywheel's angular position; β represents the angle of biped robot's leg length; r represents the length of the leg; r_0 represents the natural robot's leg length.

B. The Robot Model

Our experimental setup involves the use of a biped robot, specifically the Purple V1.0 model shown in Figure 2, which possesses 22 degrees of freedom. We denote the robot's configuration as $\boldsymbol{q} \in SE(3) \times \mathbb{R}^{16}$ and note that its arm has two joints: the upperarm and shoulder joints. The Euler-Lagrange equation is utilized to present the equations of motion for the robot, as explained in the following:

$$\boldsymbol{M}(\boldsymbol{q})\ddot{\boldsymbol{q}} + \boldsymbol{V}(\boldsymbol{q}, \dot{\boldsymbol{q}}) + \boldsymbol{G}(\boldsymbol{q}) = \boldsymbol{S}_a^T\boldsymbol{\tau} + \boldsymbol{J}_{s,p}^T\boldsymbol{F}_f \tag{4}$$

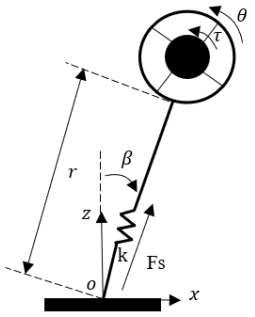

Fig. 1. The F-SLIP model.

where $\boldsymbol{M}(\boldsymbol{q})$ is the robot mass matrix ; $\boldsymbol{V}(\boldsymbol{q}, \dot{\boldsymbol{q}})$ is the Coriolis; centrifugal term; $\boldsymbol{G}(\boldsymbol{q})$ is the gravitational term; $\boldsymbol{S}_a$ is the matrix representing robot actuation ability; $\boldsymbol{\tau} \in \mathbb{R}^{16}$ is the motor torque vector; $\boldsymbol{F}_f$ is the foot contact force vector.

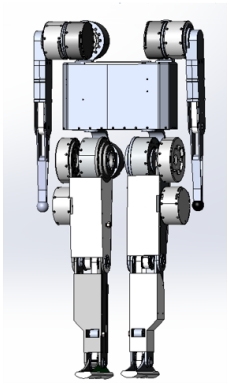

Fig. 2. Purple V1.0.

III. Trajectory Planning

For the jumping and landing phase, the general form of trajectories optimization problems is shown below:

$$\min_{\{\mathbf{x},\,\mathbf{u}\}} \; J = \min_{\{\mathbf{x},\,\mathbf{u}\}} \int_{t_0}^{t_N} L(\mathbf{x}(t), \mathbf{u}(t), t)dt \tag{5}$$

$$\text{s.t. } \dot{\mathbf{x}} = \boldsymbol{F}(\mathbf{x}(t), \mathbf{u}(t), t) \tag{6}$$

$$\boldsymbol{g}(\mathbf{x}(t), \mathbf{u}(t), t) \leq 0 \tag{7}$$

$$\boldsymbol{\psi}(\mathbf{x}(t), \mathbf{u}(t), t) = 0 \tag{8}$$

where $\mathbf{x}$ is the state vector belonging to $\boldsymbol{\mathcal{X}}$ which is the set of feasible states; $\mathbf{u}$ is the control vector belonging to $\boldsymbol{\mathcal{U}}$ which is the set of feasible input controls; scalar t is time, t_0, t_N are start and end time of a phase; L is running cost function; $\boldsymbol{F}(\boldsymbol{x}(t),\ \mathbf{u}(t), t)$ is dynamical function; $\boldsymbol{g}(\mathbf{x}(t), \mathbf{u}(t), t)$; $\boldsymbol{\psi}(\mathbf{x}(t), \mathbf{u}(t), t)$ are respectively inequation and equation constraints appied on different phases, which will be defined in the below subsections.

The program above is described by direct transcription method [18] and solved off-line using Interior Point OPTimizer (IPOPT) [19]. As for the flight phase, we plan the leg

angle according to the landing angle chosen properly.

A. Jumping Phase

In this context, the jumping phase is defined as the period of time during which the biped robot contacts with the ground until the foot leaves the ground as is $[t_0^J, t_N^J]$, J is for jumping phase. The dynamical function $\boldsymbol{F}^J$ of jumping phase is derived from Eq. (1),(2),(3), state vector $\mathbf{x}^J = [\boldsymbol{x}^J, \dot{\boldsymbol{x}}^J, \ddot{\boldsymbol{x}}^J, \theta^J, \dot{\theta}^J, \ddot{\theta}^J]^T$, control vector $\mathbf{u}^J = [\tau^J, \boldsymbol{F}_s^J]^T$, the constraints $\boldsymbol{g}^J$, $\boldsymbol{\psi}^J$ and cost functions J^J are constructed in the bellow.

1) Constraints: The velocity constraints are given by $\dot{x}^J(t_F) = \dot{x}^d$ and $\dot{z}^J(t_F) = \dot{z}^d$, where $\dot{x}^d$ and $\dot{z}^d$ are final desired COM velocities respectively that are calculated according to the ballistic equation of motion.

The given swing arm constraints determine the limitations of robot arm joints rotation, which is given by:

$$\dot{\theta}_u > \dot{\theta}^J > \dot{\theta}_l \tag{9}$$

$$\ddot{\theta}_u > \ddot{\theta}^J > \ddot{\theta}_l \tag{10}$$

where the flywheel's maximal rotational speed and acceleration are denoted by $\dot{\theta}_u$ and $\ddot{\theta}_u$ respectively, while the swing arms' minimal rotational speed and acceleration are given by $\dot{\theta}_l$ and $\ddot{\theta}_l$ respectively.

The formulation of the stability constraint, which is aimed at preventing the robot from falling, is presented below:

$$-\mu F_{s_z}^J \leq F_{s_x}^J \leq \mu F_{s_z}^J \tag{11}$$

$$0 < F_{s_z}^J \tag{12}$$

where μ is the friction coefficient.

2) Cost: To fully utilize the energy-saving benefits of swing arms [20], we have chosen to minimize the virtual energy as our optimization objective for the jumping phase:

$$J^J = \int_{t_0^J}^{t_N^J} \left(c_1 \ddot{r}^J(t) + c_2 \tau^J(t)\right) dt \tag{13}$$

where the cost proportions are indicated by the variables c_1 and c_2.

B. Flight Phase

The period of time between take-off and when the foot touches the surface of the earth is called the flight phase (F), which is defined as $[t_0^F, t_N^F]$. During this phase, the objective is to modify the body's orientation and ensure a right foothold upon landing.

We make the landing angle equal to the take-off angle $\beta^L(t_0) = \beta^F(t_F)$ according to the symmetry of motion which is the base of continuous stable motion of legged robots [1]. L is for the landing phase. Then the flight trajectory of leg angle $\beta^F(t)$ can be calculated from Eq. (1),(2),(3) by keeping $r^F(t) = r^J(t_F)$.

C. Landing Phase

The duration of the jumping motion's landing phase is described as $[t_0^L, t_N^L]$, L is for landing phase, from the time of landing which is confirmed by foot contact detection to the time when the robot reaches a state of rest, and the duration is equal to the shortest stability time when the solver can successfully solve landing optimal program.

In landing phase, it is necessary that introducing the Divergent Component of Motion (DCM) into dynamical function in order to get the desired trajectory which can rest to the balance state finally [21]. Therefore the dynamical function of landing phase $\boldsymbol{F}^L$ consists of Eq. (1),(2),(3) and Eq. (14),(15). state vector $\mathbf{x}^L = [\boldsymbol{x}^L, \dot{\boldsymbol{x}}^L, \ddot{\boldsymbol{x}}^L, \theta^L, \dot{\theta}^L, \ddot{\theta}^L, \boldsymbol{\epsilon}, \dot{\boldsymbol{\epsilon}}]^T$, control vector $\mathbf{u}^L = [\tau^L, \boldsymbol{F}_s^L]^T$

$$\boldsymbol{F}_s = s(\boldsymbol{x} - \boldsymbol{r}_{ecmp}) \tag{14}$$

$$\dot{\boldsymbol{\epsilon}} = -\frac{1}{b}\boldsymbol{x} + \frac{1}{b}\boldsymbol{\epsilon} + \frac{b}{m}\boldsymbol{F}_s \tag{15}$$

where $\boldsymbol{\epsilon} = [\epsilon_x, \epsilon_y]^T$ is DCM; $\boldsymbol{r}_{ecmp} = [p_f, 0]^T$ is Enhanced Centroidal Moment Pivot point (eCMP) [21], which is the landing foot position in this paper; $s = \frac{m}{b^2}$; $b = \sqrt{\frac{h}{g}}$; $h = z^J(t_0)$ is desired final height of landing phase.

The landing phase shares the same stability and swing arm constraints, as well as costs, as the jumping phase. We have only presented the constraints pertaining to the static configuration.

1) Constraints: To ensure that the robot stays in place above the foot as it completes the landing phase, we establish the following static configuration constraints [21] as follows:

$$\boldsymbol{x}^L(t_N^L) = \boldsymbol{r}_{ecmp} + [0, h]^T \tag{16}$$

$$\dot{\boldsymbol{x}}^L(t_N^L) = \dot{\theta}^L(t_N^L) = 0 \tag{17}$$

IV. Trajectory Tracking

In this section, we construct the WBC described as quadratic programming (QP) and solve it on-line using IPOPT [19] to track the jumping motion trajectory, and the general form of WBC is demonstrated below:

$$\min_{\{\ddot{\boldsymbol{q}}, \boldsymbol{\tau}, \boldsymbol{F}_f\}} \sum_{j=1}^{k} \|\ddot{\mathcal{A}}_p^j - \ddot{\mathcal{A}}_{c,p}^j\|_{\boldsymbol{W}_p^j} \tag{18}$$

$$\text{s.t. } \boldsymbol{M}(\boldsymbol{q})\ddot{\boldsymbol{q}} + \boldsymbol{V}(\boldsymbol{q}, \dot{\boldsymbol{q}}) + \boldsymbol{G}(\boldsymbol{q}) = \boldsymbol{S}_a^T \boldsymbol{\tau} + \boldsymbol{J}_{s,p}^T \boldsymbol{F}_f \tag{19}$$

$$\boldsymbol{J}_{s,p}(\boldsymbol{q})\ddot{\boldsymbol{q}} + \dot{\boldsymbol{J}}_{s,p}(\boldsymbol{q})\dot{\boldsymbol{q}} = 0 \tag{20}$$

$$\boldsymbol{b}_f^l < \boldsymbol{A}_{f,p}\boldsymbol{F}_f < \boldsymbol{b}_f^u \tag{21}$$

$$\boldsymbol{\tau}_l < \boldsymbol{A}_{\tau,p}\boldsymbol{\tau} < \boldsymbol{\tau}_u \tag{22}$$

$$\dot{\boldsymbol{b}}_{arm,p} < \boldsymbol{A}_{arm,p}\dot{\boldsymbol{q}} < \dot{\boldsymbol{b}}_{arm,p} \tag{23}$$

where k is number of tasks; $\ddot{\mathcal{A}}_p^j$ and $\ddot{\mathcal{A}}_{c,p}^j$ are respectively actual and commanded acceleration of the j-th controller task in phase $p = J, F, L$ which refers to jumping, flight or landing phase; $\boldsymbol{W}_p^j$ is the weight of j-th task of p phase. Eq. (19) is same as Eq. (**??**); Eq. (20) is foot contact constraint; the Jacobian matrix $\dot{\boldsymbol{J}}_{s,p}$ relates to the foot contact force; Eq. (21) is friction cone constraint; Eq. (22) is torque constraint; Eq. (23) is arms constraint restricting the motion of arm joints, which has two kinds of comparison experiments' designs in the following Section V, $\boldsymbol{A}_{arm,p}$ is the arm velocity Jacobian matrix.

A. Jumping Phase

1) 1-th task COM trajectory tracking: To achieve accurate tracking of COM trajectory during the jumping phase discussed in Section III, we describe this task in terms of joint space [22]. We relate the velocity of the COM, denoted $\dot{\mathcal{A}}_J^1$, to the rates at which the robot's joints are rotating $\dot{\boldsymbol{q}}$ through the Jacobian dynamics equation: $\dot{\mathcal{A}}_J^1 = \boldsymbol{J}_{com}\dot{\boldsymbol{q}}$, where $\boldsymbol{J}_{com}$ is the COM velocity Jacobian. However, to successfully track the task of COM trajectory, we need to determine torques that lead to joint movement acceleration $\ddot{\boldsymbol{q}}$, with $\ddot{\mathcal{A}}_J^1 = \boldsymbol{J}_{com}\ddot{\boldsymbol{q}} + \dot{\boldsymbol{J}}_{com}\dot{\boldsymbol{q}}$, such that $\ddot{\mathcal{A}}_J^1$ closely matches the desired center of mass dynamic $\ddot{\mathcal{A}}_{c,J}^1 = \ddot{\mathcal{A}}_J^{1,d} + \boldsymbol{K}_{D,com}\left(\dot{\mathcal{A}}_J^{1,d} - \dot{\mathcal{A}}_J^1\right) + \boldsymbol{K}_{P,com}\left(\mathcal{A}_J^{1,d} - \mathcal{A}_J^1\right)$ with high precision,where $\mathcal{A}_J^{1,d}$, $\dot{\mathcal{A}}_J^{1,d}$ and $\ddot{\mathcal{A}}_J^{1,d}$ represent the target values for position, speed, and acceleration of the COM in the subsection jumping phase of Section III respectively; $\boldsymbol{K}_{D,com}$ is the robot's velocity matrix of its COM ; $\boldsymbol{K}_{P,com}$ is the robot's position matrix of its COM.

2) 2-th task Attitude rotation control: Similar to the task of tracking robot's COM trajectory,we establish the centroidal pitch angular acceleration $\ddot{\mathcal{A}}_J^2 = \boldsymbol{A}_{pitch}\ddot{\boldsymbol{q}} + \dot{\boldsymbol{A}}_{pitch}\dot{\boldsymbol{q}}$, $\boldsymbol{A}_{pitch}$ [23] is the pitch centroidal angular momentum matrix. We aim to get the robot's joints torque to achieve the target joint acceleration $\dot{\boldsymbol{q}}$ which could lead $\ddot{\mathcal{A}}_J^2$ approaches 0, and doing so will prevent the robot from falling.

B. Flight Phase

During the robot's flight phase, because the robot is at the aerial state, we should remove Eq. (20),(21), and replace Eq. (19) with Eq. (24).

$$\boldsymbol{M}(\boldsymbol{q})\ddot{\boldsymbol{q}} + \boldsymbol{V}(\boldsymbol{q},\dot{\boldsymbol{q}}) + \boldsymbol{G}(\boldsymbol{q}) = \boldsymbol{S}_a^T\boldsymbol{\tau} \tag{24}$$

1) 1-th task foot trajectory tracking: In this task, we seek to determine the joint torques that will cause the robot to undergo the desired joint acceleration $\ddot{\boldsymbol{q}}$, which make the acceleration of the foot $\ddot{\mathcal{A}}_F^1 = \boldsymbol{J}_f\ddot{\boldsymbol{q}} + \dot{\boldsymbol{J}}_f\dot{\boldsymbol{q}}$ to be highly consistent with the intended movement pattern of the foot for the tracking task $\ddot{\mathcal{A}}_{c,F}^1 = \ddot{\mathcal{A}}_F^{1,d} + \boldsymbol{K}_{D,f}\left(\dot{\mathcal{A}}_F^{1,d} - \dot{\mathcal{A}}_F^1\right) + \boldsymbol{K}_{P,f}\left(\mathcal{A}_F^{1,d} - \mathcal{A}_F^1\right)$, where $\boldsymbol{J}_f$ is the foot velocity Jacobian matrix, $\ddot{\mathcal{A}}_F^{1,d}$, $\dot{\mathcal{A}}_F^{1,d}$, and $\ddot{\mathcal{A}}_F^{1,d}$ denote the target values for the position, velocity, and acceleration of robot's foot during the flight phase discussed in Section III. The foot velocity gain matrix is denoted as $\boldsymbol{K}_{D,f}$, while the foot position gain matrix is denoted as $\boldsymbol{K}_{P,f}$.

2) 2-th task foot level control: For keeping the soles of the feet level with the ground, calculation of joint torques is necessary to determine the joint acceleration $\ddot{\boldsymbol{q}}$ with $\ddot{\mathcal{A}}_F^2 = \boldsymbol{J}_{f\omega}\ddot{\boldsymbol{q}} + \dot{\boldsymbol{J}}_{f\omega}\dot{\boldsymbol{q}}$ such that $\ddot{\mathcal{A}}_F^2$ most accurately reproduces the desired task dynamics of foot level $\ddot{\mathcal{A}}_{c,F}^2 = \ddot{\mathcal{A}}_F^{2,d} + \boldsymbol{K}_{D,f\omega}\left(\dot{\mathcal{A}}_F^{2,d} - \dot{\mathcal{A}}_F^2\right) + \boldsymbol{K}_{P,f\omega}\left(\mathcal{A}_F^{2,d} - \mathcal{A}_F^2\right)$, where $\boldsymbol{J}_{f\omega}$ denote the foot angular Jacobian matrix,$\mathcal{A}_F^{2,d}$, $\dot{\mathcal{A}}_F^{2,d}$, and $\ddot{\mathcal{A}}_F^{2,d}$ represent the desired posture, angular velocity, and angular acceleration of the foot, the foot angular velocity gain matrix is denoted as $\boldsymbol{K}_{D,f\omega}$, while the foot posture gain matrix is denoted as $\boldsymbol{K}_{P,f\omega}$.

C. Landing Phase

1) 1-th task torso level control: In this task, we should find joint torques causing proper joints acceleration $\ddot{\boldsymbol{q}}$, so we could lead the torso level dynamics $\ddot{\mathcal{A}}_L^1 = \boldsymbol{J}_{t\omega}\ddot{\boldsymbol{q}} + \dot{\boldsymbol{J}}_{t\omega}\dot{\boldsymbol{q}}$ close the desire value $\ddot{\mathcal{A}}_{c,L}^1 = \ddot{\mathcal{A}}_L^{1,d} + \boldsymbol{K}_{D,t\omega}\left(\dot{\mathcal{A}}_L^{1,d} - \dot{\mathcal{A}}_L^1\right) + \boldsymbol{K}_{P,t\omega}\left(\mathcal{A}_L^{1,d} - \mathcal{A}_L^1\right)$, where $\boldsymbol{J}_{t\omega}$ is torso angular Jacobian matrix, $\mathcal{A}_L^{1,d}$, $\dot{\mathcal{A}}_L^{1,d}$ and $\ddot{\mathcal{A}}_L^{1,d}$ denote the intended values for the posture, angular velocity, and angular acceleration of the torso respectively , $\boldsymbol{K}_{D,t\omega}$ is the torso angular velocity gain matrix; $\boldsymbol{K}_{P,t\omega}$ is the torso posture gain matrix.

2) 2-th task COM trajectory tracking: The task has already been explained in the jumping phase.

V. Results and Discussion

To assess the efficiency of the suggested control method, we conducted a simulation comparison experiment using the biped robot Purple V1.0 (shown in Fig. 2). We performed several types of jumping motions in two cases: without arm-swing (NAS) and with arm-swing (AS), utilizing the Drake simulation environment [24]. The results of the simulation experiment are presented in Fig. 3, and a video of the simulations can be found at the following link: https://www.youtube.com/watch?v=fDQmcIIE8Jc.

In NAS case, the arms are limited to be static by designing $\boldsymbol{A}_{arm,p}$ of Eq. (23), and in AS case the arm can be moved just by shoulder joints while the upperarm joints are set to be Stationary through redesigning $\boldsymbol{A}_{arm,p}$ of Eq. (23).

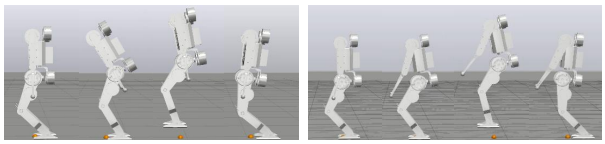

(a) **(b)**

Fig. 3. Simulation images. (a) is the jumping motion in NAS case, (b) is the jumping motion of in AS case.

A. Agility

In this section, we introduce the definition of the agility of highly dynamic motion (AHDM), which bases itself on the leaping vertically agility proposed by Haldane et al. [25]. The AHDM is defined as follows:

$$\text{AHDM} = \frac{\sqrt{h^2 + d^2}}{t_{stance} + t_{flight}} \tag{25}$$

Specifically, h stands for the vertical measurement of height that the motion reaches, d represents the straight-line distance that the motion covers, the length of the stance phase is denoted by the variable t_stance, which is the period during which the earth is in touch with the robot, and t_{flight} represents the duration of the flight phase, this is the amount of time the robot is in the air and away from the ground.

Firstly we calculate the AHDM of several kinds of jumping motions in AS and NAS cases according to COM sagittal velocity at takeoff (Fig. 4, Fig. 5) as shown in TABLE I. We

can see that compared to the NAS case, the agility in AS case can be increased by a maximum of 6%.

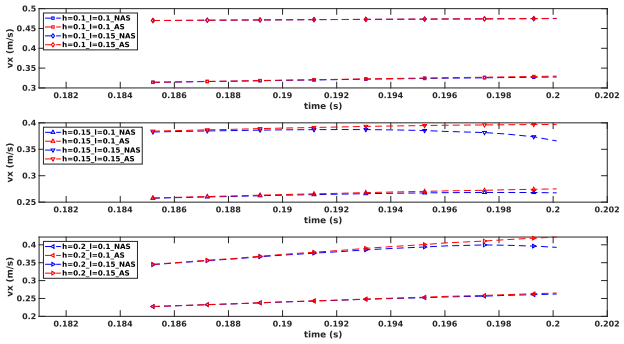

Fig. 4. vx at takeoff.

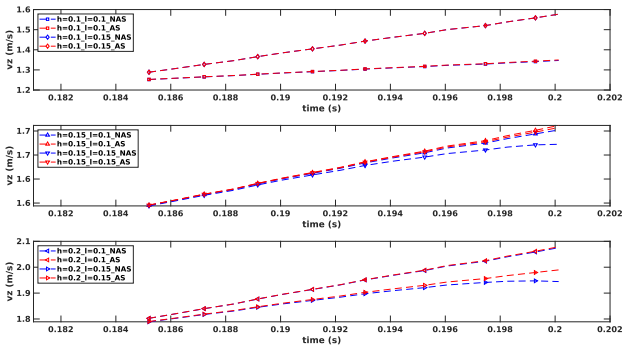

Fig. 5. vz at takeoff.

TABLE I. AHDM

case / h,d	AS	NAS
h=0.10m, d=0.10m	0.2733m/s	0.2719m/s
h=0.10m, d=0.15m	0.3809m/s	0.3807m/s
h=0.15m, d=0.10m	0.3312m/s	0.3101m/s
h=0.15m, d=0.15m	0.3701m/s	0.3502m/s
h=0.20m, d=0.10m	0.3966m/s	0.3950m/s
h=0.20m, d=0.15m	0.4369m/s	0.4156m/s

Next, we obtain plantar forces in AS and NAS cases (Fig. 6), it can be seen that plantar forces at the moment of takeoff in AS case are higher than that in NAS case.

In summary, the result coincides with the human swing arms effect 1, agility effect, during human jumping motion.

B. Stability

In this section, we define the mean peak of pitch momentum (MPPM) which is equal to the sum of pitch momentum peaks of the body divided by the number of pitch momentum peaks during the landing phase as a stability indicator.

We acquire the pitch momentum of landing phase in AS and NAS cases (Fig. 7), and then calculate the MPPM in

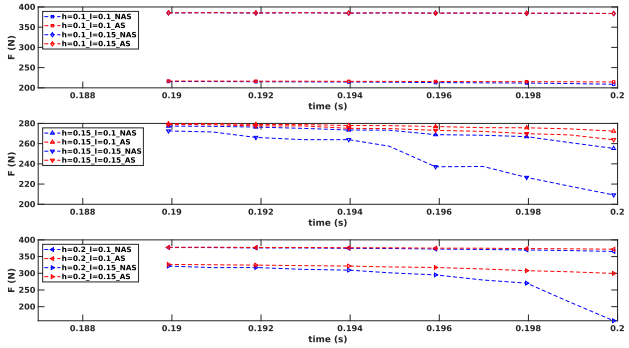

Fig. 6. Plantar forces at takeoff.

both AS and NAS cases (TABLE II), we can see that the stability is improved by an average of 30%. It is clear that in the AS scenario, the oscillation rate and intensity of pitch momentum are substantially decreased.

In conclusion, arm-swing of biped robot does enhance stability during jumping motion just like the human swing arms effect 2.

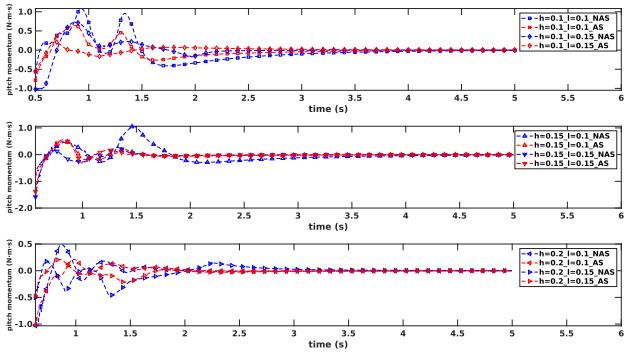

Fig. 7. Pitch momentum.

TABLE II. MPPM

case / h,d	AS	NAS
h=0.10m, d=0.10m	0.62N·m·s	0.43N·m·s
h=0.10m, d=0.15m	0.45N·m·s	0.25N·m·s
h=0.15m, d=0.10m	0.59N·m·s	0.32N·m·s
h=0.15m, d=0.15m	0.56N·m·s	0.40N·m·s
h=0.20m, d=0.10m	0.38N·m·s	0.27N·m·s
h=0.20m, d=0.15m	0.28N·m·s	0.19N·m·s

C. Energy consumption

The energy required for AS and NAS situations during jumping motions is calculated in this section where energy consumption is defined as the result of joints work. The results are presented in Figure 8. We observe that the use of arm-swing increases the overall energy consumption by an average of 6%. However, the energy consumption of the

lower limbs is reduced by an average of 25%, resulting in a total energy consumption reduction for the entire jumping motion by an average of 19% when compared to the NAS case. The increase of energy consumption caused by the introduction of arm-swing is much smaller than energy savings in the lower limbs, which has the same effect as the human swing arms.

To sum up, we can conclude that the introduction of arm-swing can significantly reduce load on lower limbs and lower overall energy consumption. This effect is the same as the human swing arms effect 3.

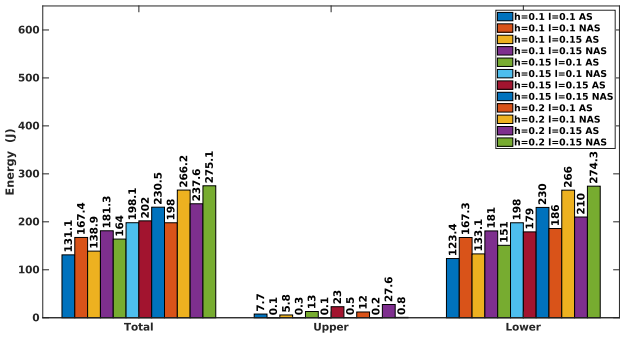

Fig. 8. Energy cost.

VI. CONCLUSION AND FUTURE WORK

The current work proposes a jumping motion control method for a biped robot equipped with swing arms and carries out multiple jumping motion experiments in both NAS and AS cases. Our analysis of the experimental results focused on three aspects: agility, stability, and energy consumption. The results suggest that introducing an arm-swing can improve all three aspects of the jumping motion. Specifically, arm-swing can enhance the agility and stability of the robot, while reducing its overall energy consumption. The proposed control strategy is able to fully utilize the advantages of arm-swing, which is consistent with the role that it plays in human motion.

In the future, we plan to further explore the theoretical basis of the proposed control strategy and validate our results on the physical robot, Purple V1.0. Additionally, we aim to apply this control strategy to more complex and highly dynamic motions such as running and continuous jumping.

REFERENCES

[1] M. H. Raibert, *Legged robots that balance*. MIT press, 1986.

[2] Raibert, Marc H, "Hopping in legged systems—modeling and simulation for the two-dimensional one-legged case," *IEEE Transactions on Systems, Man, and Cybernetics*, no. 3, pp. 451–463, 1984.

[3] W. J. Schwind, *Spring loaded inverted pendulum running: A plant model*. University of Michigan, 1998.

[4] S. H. Tamaddoni, F. Jafari, A. Meghdari, and S. Sohrabpour, "Biped hopping control bazsed on spring loaded inverted pendulum model," *International Journal of Humanoid Robotics*, vol. 7, no. 02, pp. 263–280, 2010.

[5] B.-K. Cho, J.-H. Kim, and J.-H. Oh, "Online balance controllers for a hopping and running humanoid robot," *Advanced Robotics*, vol. 25, no. 9-10, pp. 1209–1225, 2011.

[6] S. Kajita, T. Nagasaki, K. Kaneko, K. Yokoi, and K. Tanie, "A hop towards running humanoid biped," in *IEEE International Conference on Robotics and Automation, 2004. Proceedings. ICRA'04. 2004*, vol. 1. IEEE, 2004, pp. 629–635.

[7] T. Otani, K. Hashimoto, T. Isomichi, A. Natsuhara, M. Sakaguchi, Y. Kawakami, H.-o. Lim, and A. Takanishi, "Trunk motion control during the flight phase while hopping considering angular momentum of a humanoid," *Advanced Robotics*, vol. 32, no. 22, pp. 1197–1206, 2018.

[8] A. Lees, J. Vanrenterghem, and D. De Clercq, "Understanding how an arm swing enhances performance in the vertical jump," *Journal of biomechanics*, vol. 37, no. 12, pp. 1929–1940, 2004.

[9] B. M. Ashby and S. L. Delp, "Optimal control simulations reveal mechanisms by which arm movement improves standing long jump performance," *Journal of biomechanics*, vol. 39, no. 9, pp. 1726–1734, 2006.

[10] M. Pijnappels, I. Kingma, D. Wezenberg, G. Reurink, and J. H. Van Dieën, "Armed against falls: the contribution of arm movements to balance recovery after tripping," *Experimental brain research*, vol. 201, no. 4, pp. 689–699, 2010.

[11] P. Meyns, S. M. Bruijn, and J. Duysens, "The how and why of arm swing during human walking," *Gait & posture*, vol. 38, no. 4, pp. 555–562, 2013.

[12] M. L. De Graaf, J. Hubert, H. Houdijk, and S. M. Bruijn, "Influence of arm swing on cost of transport during walking," *Biology open*, vol. 8, no. 6, p. bio039263, 2019.

[13] A. Miyata, S. Miyahara, and D. N. Nenchev, "Walking with arm swinging and pelvis rotation generated with the relative angular acceleration," *IEEE Robotics and Automation Letters*, vol. 5, no. 1, pp. 151–158, 2019.

[14] B. Park, M.-J. Kim, E. Sung, J. Kim, and J. Park, "Whole-body walking pattern using pelvis-rotation for long stride and arm swing for yaw angular momentum compensation," in *2020 IEEE-RAS 20th International Conference on Humanoid Robots (Humanoids)*. IEEE, 2021, pp. 47–52.

[15] H. Mineshita, T. Otani, M. Sakaguchi, Y. Kawakami, H. Lim, and A. Takanishi, "Jumping motion generation for humanoid robot using arm swing effectively and changing in foot contact status," in *2020 IEEE/RSJ International Conference on Intelligent Robots and Systems (IROS)*. IEEE, 2020, pp. 3823–3828.

[16] J. Pratt, J. Carff, S. Drakunov, and A. Goswami, "Capture point: A step toward humanoid push recovery," in *2006 6th IEEE-RAS international conference on humanoid robots*. IEEE, 2006, pp. 200–207.

[17] K. Bouyarmane, K. Chappellet, J. Vaillant, and A. Kheddar, "Quadratic programming for multirobot and task-space force control," *IEEE Transactions on Robotics*, vol. 35, no. 1, pp. 64–77, 2018.

[18] P. J. Enright and B. A. Conway, "Discrete approximations to optimal trajectories using direct transcription and nonlinear programming," *Journal of Guidance, Control, and Dynamics*, vol. 15, no. 4, pp. 994–1002, 1992.

[19] A. Wächter and L. T. Biegler, "On the implementation of an interior-point filter line-search algorithm for large-scale nonlinear programming," *Mathematical programming*, vol. 106, no. 1, pp. 25–57, 2006.

[20] B. Kaddar, Y. Aoustin, and C. Chevallereau, "Arm swing effects on walking bipedal gaits composed of impact, single and double support phases," *Robotics and Autonomous Systems*, vol. 66, pp. 104–115, 2015.

[21] J. Englsberger, C. Ott, and A. Albu-Schäffer, "Three-dimensional bipedal walking control using divergent component of motion," in *2013 IEEE/RSJ International Conference on Intelligent Robots and Systems*. IEEE, 2013, pp. 2600–2607.

[22] O. Khatib, "A unified approach for motion and force control of robot manipulators: The operational space formulation," *IEEE Journal on Robotics and Automation*, vol. 3, no. 1, pp. 43–53, 1987.

[23] D. E. Orin and A. Goswami, "Centroidal momentum matrix of a humanoid robot: Structure and properties," in *2008 IEEE/RSJ International Conference on Intelligent Robots and Systems*. IEEE, 2008, pp. 653–659.

[24] R. Tedrake and the Drake Development Team, "Drake: Model-based design and verification for robotics," 2019. [Online]. Available: https://drake.mit.edu

[25] D. W. Haldane, M. M. Plecnik, J. K. Yim, and R. S. Fearing, "Robotic vertical jumping agility via series-elastic power modulation," *Science Robotics*, vol. 1, no. 1, p. eaag2048, 2016.